ROYAL SOCIETY
OF CHEMISTRY

REVIEW

Check for updates

Advancements in theoretical and experimental investigations on diamane materials

Bowen Liu,†[a,b] Emilia Emmanuel, ID †[a,b] Tao Liang*[c] and Bin Wang ID *[a,b]

Technology-driven modern civilization demands new materials as its backbone. Consequently, based on intense research, a promising candidate, diamane, which is a two-dimensional (2D) form of diamond with a bilayer sp^3 carbon nanostructure, has been proposed and recently achieved from bi-layer graphene (BLG) or few-layer graphene (FLG) through high-pressure technology or surface chemical adsorption. This material has been reported to possess a tunable bandgap, excellent heat transfer ability, ultralow friction, and high natural frequency, which can be a potential asset for cutting-edge technological applications, including quantum devices, photonics, nano-electrical devices, and even space technologies. In this review, following the history of the development of diamane, we summarize the recent theoretical and experimental studies on diamane in its pristine form and functionalized with substituents (H–, F–, Cl–, and OH–) in terms of atomic structure, synthesis strategies, physical properties, and potential technological applications. Also, the current challenges and future opportunities for the further development of diamane are discussed. As a young material with great potential but limited experimental research, there is still great space for its exploration.

1. Introduction

Diamond and graphite are two allotropes of carbon. Graphite is a soft and opaque semimetal, whereas diamond is hard, thermally conductive, chemically inert, and optically transparent.[1–3] When graphite is reduced to a monolayer thickness (graphene), it presents abundant and novel physical properties, such as high carrier mobility,[4] half-integer quantum Hall effect,[5–7] and unconventional superconductivity.[8,9] Thus, the preparation of atomically thin diamond film has also been attempted;[10–22] however, in contrast to the van der Waals interaction in graphite, the strong carbon–carbon covalent bond in three directions hinders the direct top-down exfoliation of bulk diamond. Atomic-layer C_2H was named "diamane" by Chernozatonskii *et al.*[23] and their prediction that diamane possesses excellent properties and technological promise, thus it has attracted increasing interest. Basically, authentic diamane consists of two crystalline sp^3-bonded layers of carbon (sp^3-C), half of which are hydrogenated, while the other half bonds the two layers together.[23] However, atomically

thin diamane is considered to be unstable in the clean state (without light atom passivation, for example, H or F) under normal conditions given that diamond forms a three-dimensional crystalline structure and will lose its chemical stability when thinned down to the thickness of the unit cell of diamond owing to the presence of dangling sp^3 bonds. Surface chemical functionalization with unique species, such as H–, F–, and Cl– atoms and –OH groups, was deemed to be necessary for the 2D diamond structure to be thermodynamically stabilized.[24–31] In this case, both hydrogenation and fluorination of its surface were attempted experimentally[13,30] and the structures were labeled as diamane and F-diamane (FD) (two-side functionalized bilayer and few-layer graphene) discussed in literature,[32–34] respectively, to distinguish them from another diamane-like material called diamone, which is formed by the light atom passivation of one side of BLG.[35]

The synthesis routes for diamane can be roughly classified into two major categories, where one route is surface functionalization-induced interlayer carbon atoms bonding in bilayer or multilayer graphene under atmosphere pressure, while the other route is to convert bilayer or multilayer graphene to diamane directly by applying high pressure, similar to the transformation of graphite to diamond. The former route generates functionalized diamane, which is stable with heteroatoms on its surface, were the products may be diamondol (when the topmost surface is covered with –OH groups),[10] diamanoid[19,36] (crystalline sp^3-bonded 2D carbon materials either similar to diamane but composed of more

*[a]CAS Key Laboratory of Nanosystem and Hierarchical Fabrication, National Center for Nanoscience and Technology (NCNST), Beijing 100190, China.
E-mail: wangb@nanoctr.cn*
[b]University of Chinese Academy of Sciences, Beijing 100049, China
[c]Hangzhou Institute for Advanced Study, University of Chinese Academy of Sciences, Hangzhou, China. E-mail: liangtao@ucas.ac.cn
†These authors made equal major contributions to this work.

than two layers or with only one outer hydrogenated (or fluorinated) layer regardless of the number of layers) or diamondene[14] (a mixture, diamondized by hydroxyl groups and hydrogens) depending on the surface functional atoms and the layers of graphene precursor. In contrast, the latter route can usually be used to obtain clean diamane (CD) with carbon atoms only.

To date, there are only a few reviews in the literature discussing the emerging material diamane. Piazza et al. summarized the progress on diamane and diamanoid thin films obtained via pressure-less synthesis,[37] and subsequently Sorokin et al. provided a mini review on the stabilization of diamond and its corresponding structure–property relationships.[33] Tiwari et al. and Qin et al. presented reviews on the recent progress of diamanes and diamanoids for emerging techniques.[38,39] In this review, we categorize the history of the development of diamane, which has not been provided in previous reviews, and mainly focus on the experimental results associated with its synthesis processes and several key pro-perties obtained by theoretical simulations. By summarizing the exciting works on the synthesis and understanding diamane and its derivatives, this review may help more researchers focus on this rising star material and accelerate its research toward potential applications in optics, electronics, and mechanics.

2. Development of diamane

Diamane is a type of 2D material developed following the research on graphene. Although P.R. Wallace theoretically discovered graphene in 1947,[40] the experimentation for its identification and isolation was only reported in 2004 by A. Geim and K. Novoselov.[41] Since then, the research on 2D structures continued, and 2009, a new C_2H nanostructure named diamane was studied theoretically by covalently bonding hydrogen atoms on the outer surfaces of BLG, while carbons are also bonded between the neighboring layers.[23]
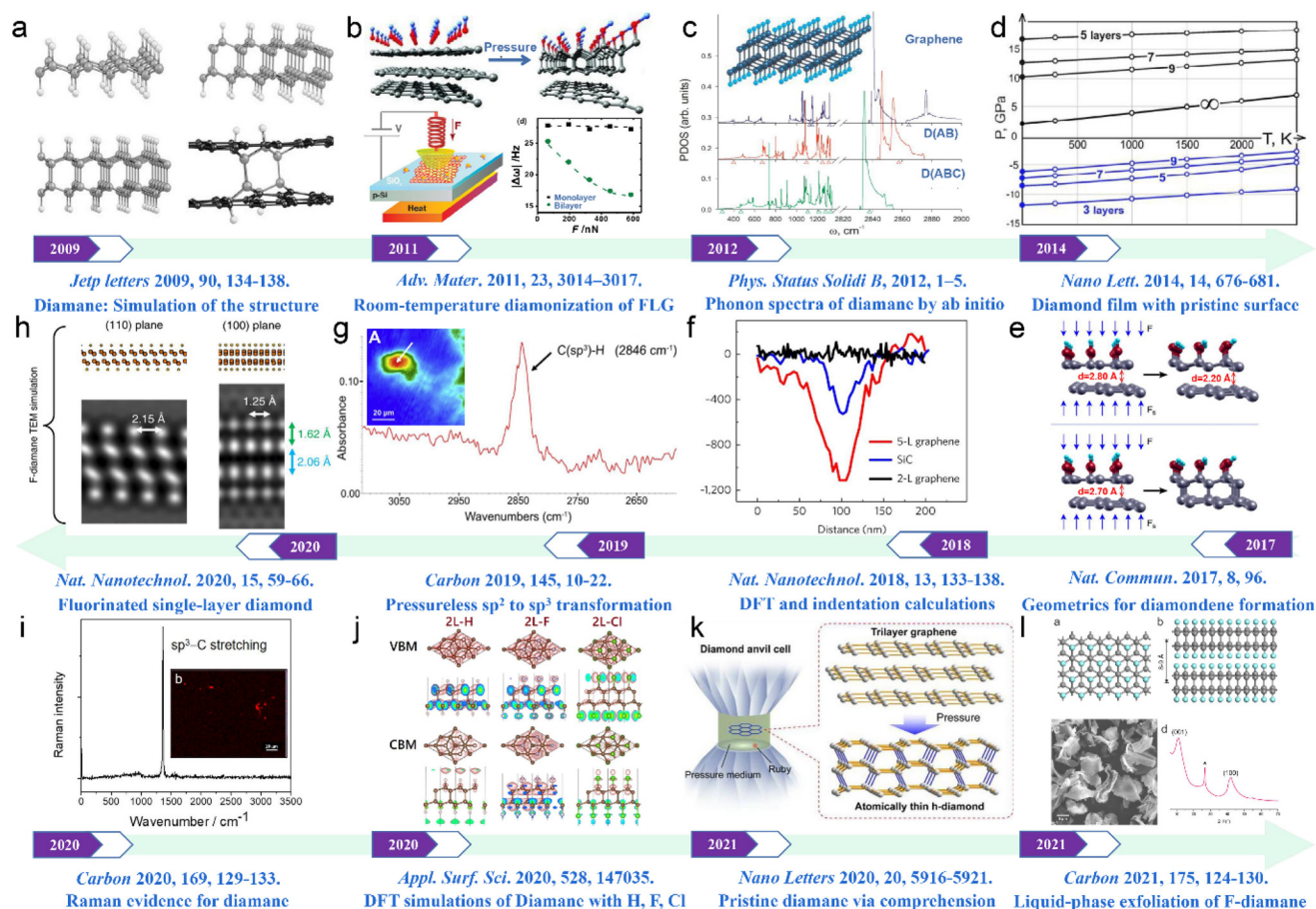

Fig. 1 Schematic representation of key works during the development of diamane research. (a) Reproduced with permission.[23] Copyright 2009, Springer Nature. (b) Reproduced with permission.[10] Copyright 2011, Wiley-VCH. (c) Reproduced with permission.[43] Copyright 2012, Wiley-VCH. (d) Reproduced with permission.[26] Copyright 2014, the American Chemical Society. (e) Reproduced with permission.[14] Copyright 2017, Springer Nature. (f) Reproduced with permission.[15] Copyright 2018, Springer Nature. (g) Reproduced with permission.[16] Copyright 2019, Elsevier B.V. (h) Reproduced with permission.[30] Copyright 2020, Springer Nature. (i) Reproduced with permission.[18] Copyright 2020, Elsevier B.V. (j) Reproduced with permission.[31] Copyright 2020, Elsevier B.V. (k) Reproduced with permission.[17] Copyright 2020, the American Chemical Society. (l) Reproduced with permission.[44] Copyright 2021, Elsevier B.V.

Subsequently, efforts have been devoted to the simulation of diamane structures and properties, and also possible ways to synthesize diamane and its derivatives experimentally (Fig. 1). Over the years, experimental evidence has demonstrated that the chemical functionalization of BLG with specific chemical groups and atoms is necessary to stabilize the 2D structure of diamond films.[16,22,30,42] The simulated properties of diamane have also shown its considerable potential for use in diverse fields such as electronics and high-strength composites desirable for thin safety coating in aerospace.[16] Together with the development of diamane research, as shown in Fig. 1, its experimental synthesis and the theoretical prediction of physical properties are introduced in the following sections.

2.1 Early theoretical studies on functionalized diamane

The use of BLG in the synthesis of diamond-like carbon has demonstrated the potential of diamanes as nanostructured materials, with the subsequent development of nanodevices. Traditionally, the conversion of multilayer graphene to diamane requires extreme temperature and pressure conditions to overcome the energy barrier for the transformation of the sp^2 bond to sp^3 type.[28,45,46] However, surface chemical functionalization with unique chemical radicals has been

shown to reduce the energy barrier of this conversion.[10,24] The electronic properties are susceptible to change according to the variation in the graphitic carbon skeleton. To achieve the desired structures in diamane, the main consideration is to choose the appropriate functional groups in terms of their molecular or atomic states. The type of structural deformation, the quantity of sp^3 carbon, the type of heteroatoms and the location of hydrogenated graphene all contribute significantly to the uniqueness of these structures.[47] In this regard, the hydrogenation of BLG was attempted theoretically. Correspondingly, the uniform adsorption of atomic hydrogen on BLG yields strong chemical bonds between the layers of the material, which significantly stabilize the structure of diamane by removing van der Waal forces. It should be specified that when the two outer surfaces of BLG are functionalized with homoatoms, the product is named non-Janus diamane, such as diamane (hydrogen atoms bonded on both sides). The atomic structure, dynamic stability, and optical and electronic properties of diamane have been predicted by density functional theory (DFT) calculations using the Vienna *Ab initio* Simulation Package (VASP).[48] The results of the atomic structure study showed that diamane is similar to graphane, which is fully hydrogenated single-layer graphene (SLG) (Fig. 2(a1)).
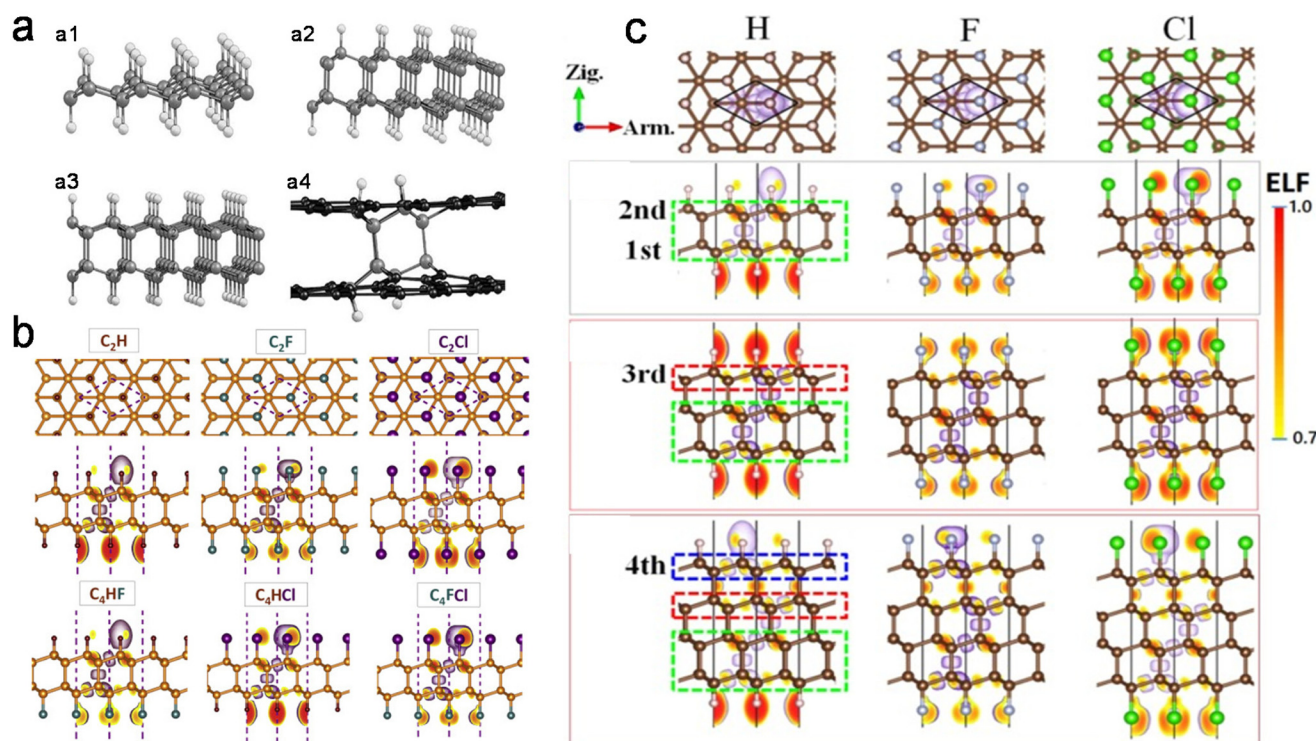
Fig. 2 (a) Atomic structures of (a1) graphane, (a2) diamane, and (a3) diamane II (AA-diamane). (a4) Scheme of the formation of a diamane nucleus in an initial AB-stacked BLG: hydrogen atoms settle from two sides and initiate the "bonding" of carbon atoms located over each other in neighboring carbon layers. Reproduced with permission.[23] Copyright 2009, Springer Nature. (b) Atomic structure of the considered non-Janus and Janus diamane nanosheets. Iso-surfaces (set at 0.7) illustrate the electron localization function within the unit cell. Reproduced with permission.[49] Copyright 2020, Elsevier B.V. (c) Top and side views for the atomic structure of diamane nanosheets with different functional groups (H, F, and Cl) and layers of carbon atoms (2L, 3L, and 4L). Contours illustrate the electron localization function (ELF) in the unit-cell. Mechanical properties are examined along the armchair (Arm.) and zigzag (Zig.) directions, as shown in the top views. Reproduced with permission.[31] Copyright 2020, Elsevier B.V.

Specifically, the structure of graphane predicted by Sofo et al. is formed by a single layer of sp[3]-bonded carbon with a hexagonal network, where each carbon is bonded to one hydrogen above and below the surface alternately.[2] The structures of diamane, as shown in Fig. 2(a2) and (a3), are derived from AB (Bernal) and AA (lonsdaleite)-stacked BLG, which are called "diamane" and its isomer "diamane II", respectively, and the neighboring carbon atoms in each layer are bonded covalently. A schematic of the initial formation of the diamane nucleus from an AB-stacked BLG is shown in Fig. 2(a4) with the hydrogen atoms chemically adsorbed on both sides of BLG under specific conditions (pressure and temperature of the hydrogen gas in discharge hydrogen plasma).[23] Theoretical results suggest that diamane is more stable than graphane and it has a direct bandgap (E_g) of 3.12 eV. According to the estimated elastic constants of 238, 449, and 715 N m^{-1} for graphene, graphane, and diamane, respectively, diamane is perhaps the strongest among the thin carbons, which is somewhat similar to the diamond crystals, as reported in the literature.[23,24]

In addition, besides non-Janus diamane, there is a possibility that Janus diamane nano-membranes can be fabricated with the outer surface of BLG functionalized with heteroatoms.[49] The generalized gradient approximation (GGA) with Perdew–Burke–Ernzerhof revised for solids (PBEsol)[50] was used to investigate the atomic structure and dynamic stability of non-Janus C_2H, C_2F, and C_2Cl diamane and their Janus counterparts of C_4HF, C_4HCl, and C_4FCl, respectively. The top and side views of the geometry-optimized diamane monolayers considered are shown in Fig. 2b. Electron localization function (ELF)[51] was used to investigate the type of chemical bond, which was found to be covalently bonded throughout the diamane nanosheets, and the thermal stability was calculated through ab initio molecular dynamics (AIMD) simulations. Furthermore, elastic modulus investigation showed that these nanosheets exhibit an in-plane isotropic elasticity property. Using PBEsol and the hybrid HSE06 functional,[52] the electronic band structure was found to exhibit semiconducting features with a direct HSE06 (PBEsol) bandgap. Similarly, the simulation results of the C_4HCl Janus diamane structure showed that it has higher thermal conductivity than non-Janus C_2Cl. Also, Janus C_4HF yields lower and higher thermal conductivity than its non-Janus C_2H and C_2F counterparts, respectively. Mortazavi et al. used the PBEsol method to describe the atomic structure in functionalized diamane, showing energy-minimized H-, F-, and Cl-diamane (ClD) nanosheets with a graphene-like hexagonal atomic lattice, as shown in Fig. 2c.[31] Meanwhile, these structures were described with respect to the functional group and number of carbon layers. The iso-surface densities (ELF = 0.7) around the center of C–C bonds, and also along the functional groups confirm the covalent interactions throughout these 2D materials.[31] Phonon dispersions and ab initio molecular dynamics results confirmed that the H-, F-, and Cl-diamane nanosheets exhibit good stability. The extensive theoretical research results provide a comprehensive perspective on the key properties of diamane from stability and mechanics to electronics/optics,

and further provide persuasive guidance for experimental exploration.

2.2 Experimental research on diamane

2.2.1 Hydrogenated and hydroxylated diamane.
The research history of diamane is short, and most of the studies are based on theoretical simulations.[11,43] To date, there still lack of a commonly accepted experimental methods to produce high-quality or high-yield diamane materials, such as the physical/chemical exfoliation[53] and chemical vapor deposition methods used for the synthesis of graphene. Rajasekaran et al.[13] reported some experimental evidence that hydrogen adsorption can induce the partial phase transition of few-layer graphene (FLG) to a diamond-like structure on a Pt (111) surface. The surface adsorption of hydrogen induces a hybridization change of carbon from the sp[2] to sp[3] bond symmetry, which propagates through the graphene layers, resulting in interlayer carbon bond formation, as stated by the authors. However, it should be noted out that the empirical evidence presented by them was insufficient, such as Raman spectroscopy and transmission electron microscopy (TEM) measurements. In this case, it was only in 2019 that persuasive empirical evidence, particularly Raman spectroscopy, for conversion of sp[2] to sp[3] hybridization in FLG was reported.[16] Piazza et al. studied the hydrogenation of FLG by chemisorption of H generated from the dissociation of H_2 in a hot filament reactor at low temperature and low pressure, where the successful conversion from sp[2]-C to sp[3]-C in the hydrogenated FLG was verified by UV Raman spectroscopy.[16]

Nevertheless, insufficient evidence was provided in these reports to claim the production of diamane from BLG instead of diamane/graphene hybrids. Research showed that once the number of graphene layers in the starting FLG is higher than 2–3, the sp[2]-C to sp[3]-C conversion happens partially due to the prevalent Bernal stacking sequence. Partially hydrogenated FLG is commonly called diamanoid, as shown in Fig. 3a.[19] The first proof of the successful synthesis of diamane from BLG and evidence of UV Raman spectra together with TEM characterization were reported by Piazza et al.[18] Micro-Raman mapping was performed before and after (Fig. 3(b1) and (b2)) the hydrogenation process promoted by hot filaments, respectively. The spectrum of BLG showed a normal sharp G peak at around 1582 cm^{-1} before hydrogenation owing to the extended bonds of all pairs of sp[2]-C in the graphene sheets. In contrast, significant changes were observed in the Raman spectrum after the hydrogenation process, as follows: (i) the G peak was no longer detected and (ii) only the sp[3]-C stretching signal appeared; clarifying the full sp[2]-C to sp[3]-C conversion, that is, the full conversion of BLG into genuine diamane, at least at the position of the Raman laser spot.

Similar to hydrogenation, hydroxyl groups can also be used as chemical radicals to stabilize the diamondization of FLG, which is called diamondol, with the topmost of FLG covered with hydroxyl groups and no further modification of the eventual additional underlying graphene layers. Barboza et al. reported how the pressure applied by means of the tip of a
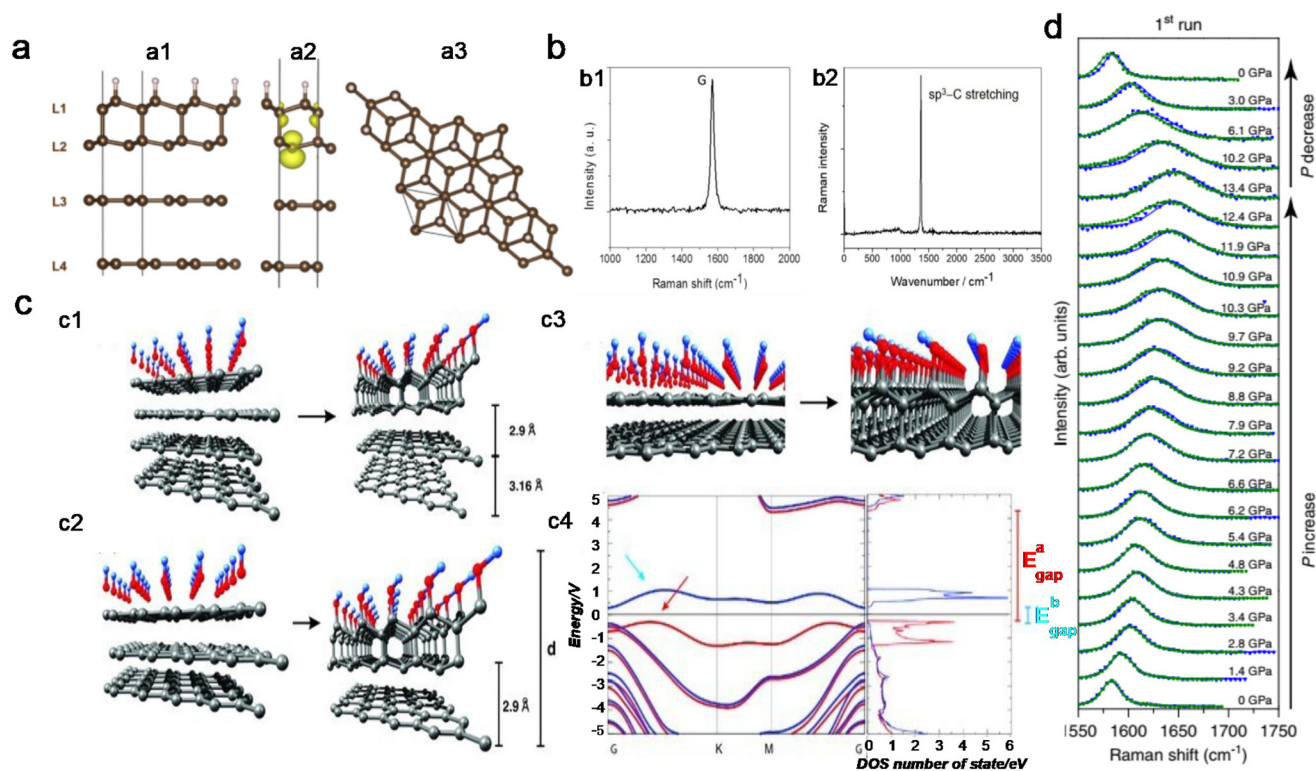
Fig. 3 (a), (a1) and (a2) two-side view and (a3) top view of the partially hydrogenated few-layer graphene (FLG) used in DFT calculations with ABBA stacking. Reproduced with permission.[19] Copyright 2020, Elsevier B.V. (b) Raman spectra (at 244 nm) of FLG (b1) before and (b2) after hydrogenation. Reproduced with permission.[18] Copyright 2020, Elsevier B.V. (c) Initial and optimized geometries for (c1) four, (c2) three, and (c3) two graphene layers. (c4) Spin-dependent electronic dispersion and the density of states (DOS) for the unit cell of the final structure in (c3). Reproduced with permission.[10] Copyright 2011, Wiley-VCH. (d) Evolution of the G band with increasing pressure (up to ≈14 GPa) using water as the pressure transmission medium. The respective applied pressure is indicated on the right side of each respective spectrum. Two spectra are shown for each pressure level, one obtained with an excitation laser energy EL = 2.33 eV (green symbols), and the other with EL = 2.54 eV (blue symbols). The solid lines are the Voigt fit to the experimental data. Reproduced with permission.[14] Copyright 2017, Springer Nature.

scanning probe microscope (SPM) to bilayer and multilayer graphene samples induced a structural change in water medium.[10] The amount of pressure-dependent injected charge manipulated with electric force microscopy (EFM) was found to be substantially reduced and this observation was not observed in a dry climate. The diamondization of the top graphene surface was assumed to be due to the hydroxyl group given by the water pressure, and the structure could not be sustained at ambient pressure. The hydroxyl-induced surface was also demonstrated spontaneously in an *ab initio* calculation. Fig. 3(c1) shows the initial and final configurations of an unconstrained geometry optimization process, where the initial geometry is a four-layer graphene with one hydroxyl group placed above each carbon atom at the top layer sublattices. Fig. 3(c2) and (c3) show the corresponding optimized structures obtained with three- and two-layer graphene in the initial geometry and (c4) represents the spin-dependent electronic dispersion and the density of states (DOS) for the unit cell of the final structure in (c3). Consequently, the structure obtained was proven to have a ferromagnetic insulator phase with various bandgap energies for each spin with regard to the stacking layers. This phenomenon, which was observed as a

reversible compression-induced charging inhibition of bilayer and multilayer graphene, presented theoretical and experimental evidence for the room-temperature diamondization of few-layer graphene.

Furthermore, spectroscopic evidence of the formation of a hydroxylated 2D-diamond structure, denoted as diamondene (actually a mixture, diamondized by hydroxyl groups and hydrogens) was provided. Martins *et al.* conducted experiments with high pressure on the top of BLG in a diamond anvil cell (DAC).[14] Water was used as the experimental supplier of hydroxyl or hydrogen atoms and the pressure transmission medium (PTM). BLG was synthesized *via* chemical vapor deposition and transferred to a Teflon substrate. The substrate did not react with the precursor graphene and could avoid the functionalization of the bottom carbon atoms. Through Raman spectroscopy measurement, it was found that the hybridization of carbon in the sample existed in a mixed state of sp^2 and sp^3, and an enhancement in the G band occurred as the pressure increased, as shown in Fig. 3d. DFT results showed that diamane was formed at the pressure of 4–5 GPa. The DAC-assisted high pressure experiments induced the as-observed transformation of carbon structures and enabled the

investigation of some intrinsic physical properties of diamane, although the obtained structure is reported to be unstable when being exposed to ambient condition, and thus is not a universal material preparation method.

2.2.2 Fluorinated diamane. A diamond-like structure called F-diamane (FD) can be formed by functionalizing the surface of BLG/FLG with fluorine atoms. The fluorination of graphene was reported to enable easier characterization in experiments compared with the graphene hydrogenation reaction.[30] FD was obtained under moderate conditions at near room temperature and low/atmospheric pressure using xenon difluoride (XeF_2) vapour as the source of fluorine, while the thermal stability was better than diamane. This is because the formation energy in the case of fluorination is significantly lower (almost 1 eV) than in the case of hydrogen chemisorption, which can be attributed to the weaker bond in F_2 compared with the H_2 molecule and the reduced configuration space, as reported in the literature.[54] Also, due to the strongly polarized C–F bonds compare to C–H bonds, fluorine can be directly identified by conventional characterization methods such as XPS, energy dispersive X-ray spectroscopy (EDX) and electron energy loss spectroscopy (EELS). *Ab initio* studies on fluorinated graphene have been carried out to compare the properties of fluorinated graphene bilayer to that of graphene, diamane, and one- or two-layered hydrogenated graphene.[23,24,54] FD is an ultrathin material with a direct bandgap larger than diamane. For instance, the estimated bandgap of FD was found to be over 30% that of diamane. The electronic properties could also be modulated with a decrease in bandgap by means of applied strain or fluorine vacancy (VF), especially a bandgap transition, which was found to be from direct to indirect at the case of tensile strain of 2.7%.[55] In addition, its elastic module is reported to be equivalent to that of graphene and higher than most other 2D materials.[56]

"Top-down" and "bottom-up" approaches have been used to prepare FD in experiments. Experimental proof of the stable FD developed over a wide area at atmospheric pressure was provided by Bakharev *et al.*[30] The experimental process was performed by flowing xenon difluoride (XeF_2) gas over a BLG sample on a single-crystal CuNi (111) substrate for several hours at ambient pressure. The reaction between graphene and XeF_2 forces the carbon atoms in BLG to bond with fluorine atoms in an sp^3 configuration, resulting in the formation of interlayer carbon–carbon bonds in FD. There are two possible structures of the obtained samples, where the first structure in shown in Fig. 4(a1) with sp^3-hybridized carbon atoms participating in the interlayer C–C and surface C–F bonds, which is characterized as single diamond-layer (FD), and the second structure (Fig. 4(a2)) with the fluorine atoms bonding on both sides of each sheet where no interlayer linkage happens.[30]

Interlayer C–C linkages stabilize the local structure by forming covalent bonds between the F atoms at the interface and bottom layer. In this work, the structural information and transition dynamics were demonstrated by various techniques, and the most direct evidence was given by high-resolution transmission electron microscopy (TEM), as shown in Fig. 4b. An obvious variation in interlayer distance and the formation of C–F bonds on two sides of graphene were observed. Similarly, applying XeF_2 gas as the source of fluorine for fluorination, Son *et al.* demonstrated a method to fabricate single- or double-sided fluorinated BLG by tailoring the substrate interactions, where both the top and bottom surfaces of BLG on the rough silicon dioxide (SiO_2) are fluorinated. Meanwhile, only the top surface of graphene on hexagonal boron nitride (hBN) is fluorinated, providing an interesting strategy for the fabrication of FD (Fig. 4c).[57] Unlike the above-mentioned "bottom-up" manner, which has a rigid process control and relatively high cost, liquid phase exfoliation as a typical "top-down" process is a simple and versatile means to produce ultrathin layers in large quantities. Chen *et al.* implemented a new fabrication method with sonication-assisted exfoliation of $(C_2F)_n$ in solvents to synthesize few-layer FD sheets with a high yield (Fig. 4d).[44] The TEM images showed an interlayer space of ~0.90 nm, in comparison to that of ~0.34 nm for the pristine graphene layers, suggesting the formation of FD materials with just a few layers. Thus, this liquid exfoliation method can possibly be a future approach to produce large amount diamane materials for potential applications.

2.2.3 Clean diamane. Chemical methods have been demonstrated to have the capability to realize the formation of interlayer carbon bonds, but the introduction of heteroatoms and unsaturated sp^2-to-sp^3 transformation make them unsuitable to produce clean diamane (CD) materials. In early works, the high-pressure phase transition of pristine FLG was investigated in a DAC under hydrostatic and non-hydrostatic conditions, which could be used to make CD without introducing hydrogen atoms. By combining X-ray diffraction and Raman spectroscopy results, the strain dependence of the normalized G-band of the present seven-layered graphene under hydrostatic compression in comparison with that measured in non-hydrostatic tension by four-point bending measurements, as shown in Fig. 5a. Notably, the slope changed at around 16 GPa, signifying the deviation of the two-dimensional layer structure of graphene and the loss of its long-range order, which indicates that the interlayer sp^3 C–C bonds were possibly formed in seven-layered graphene at 16 GPa with partial sp^2 bonds.[58] Subsequently, the thermodynamic steps for the conversion of 2–8 layers of graphene to CD were studied (Fig. 5b),[26] which showed that diamond is difficult to be nucleated due to the graphitization effect when its number of layers is two. The CD becomes metastable when the number of layers is greater than five, where a semi-metal to semiconductor transition occurs and phase transition pressure increases when the number of layers increases. In another case, CD with three or more carbon layers was synthesized *via* the diamondization of a mechanically exfoliated trilayer and thicker graphene *via* compression (Fig. 5c).[17] The diamondization process is usually accompanied by the opening of an energy gap and dramatic increase in resistance. The study showed that CD can be synthesized through the compression of tri-layer and thicker graphene up to 20 GPa, which can then
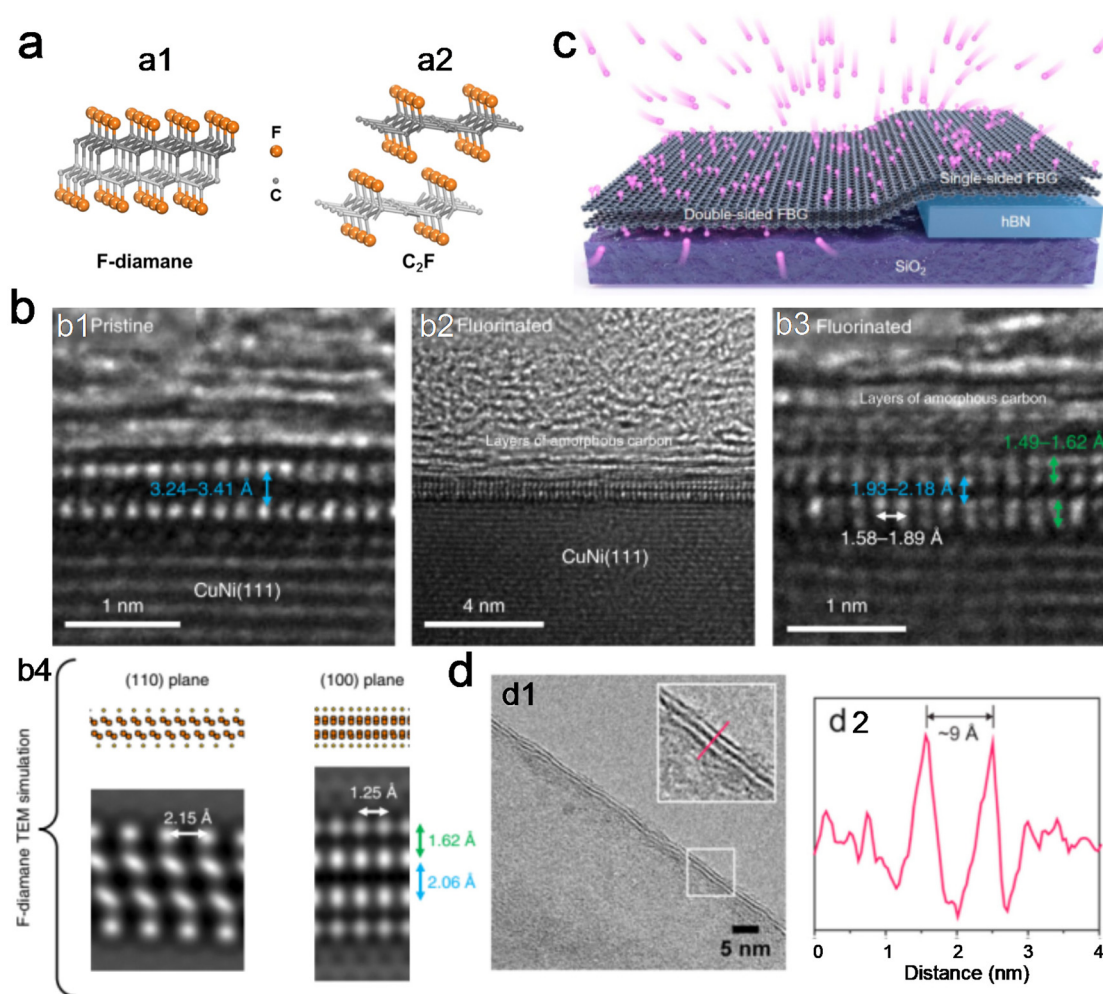
Fig. 4 Experimental evidence of the fluorinated diamane (FD). (a) Ball and stick models of (a1) FD and (a2) the C_2F structure without interlayer C−C bonds. (b) TEM study of FD on CuNi (111) surface. High-resolution cross-sectional TEM images of as-grown pristine graphene bilayer (b1) and sample (b2, b3, and b4) HR-TEM images of FD. Reproduced with permission.[30] Copyright 2020, Springer Nature. (c) Schematic illustration of the fabrication process of the BLG device exposure to XeF_2 gas. Reproduced with permission.[57] Copyright 2021, the American Chemical Society. (d) Magnified TEM image of exfoliated $(C_2F)_n$ platelet, showing the edge of the platelet. The inset in (d1) shows a magnified image of the edge. (d2) Plot of the profile along the line in (d1) inset, indicating a ~0.9 nm interlayer distance. Reproduced with permission.[44] Copyright 2021, Elsevier B.V.

be maintained to 1.0 GPa after decompression. The phase transition pressure of pristine graphene estimated by the measurement of resistance depends greatly on the number of graphene layers, that is, a higher pressure in thinner samples (Fig. 5d).

The first practical demonstration of the transformation of BLG into diamond-like ultrahard structures under ambient condition was reported by Gao *et al.*, showing that at room temperature and after nano-indentation through the tip of the atomic force microscopy (AFM) probe, the BLG on SiC (0001) exhibits a transverse stiffness and hardness comparable to diamond and the electrical conductivity shows a reversible drop upon indentation.[15] DFT calculations suggested that upon compression, the BLG film transformed into a diamond-like film, producing both elastic deformations and sp^2 to sp^3 chemical changes. In brief, current studies showed that extre-

mely high pressure is necessary for the fabrication of high-quality CD if there are no additional chemical moieties such as −H and −F to stabilize the dangling bonds on the surface of the carbon layers. However, the expensive instrumental setup, and critically the unstable CD structure when released to atmospheric pressure present challenges for the large-scale fabrication of CD.

3. Properties and potential applications of diamane

According to computational studies, diamane displays the electronic structure of semiconductors, with a direct bandgap,[24] and its bandgap is also tunable based on its thickness, functional group type, and conformation.[59] These
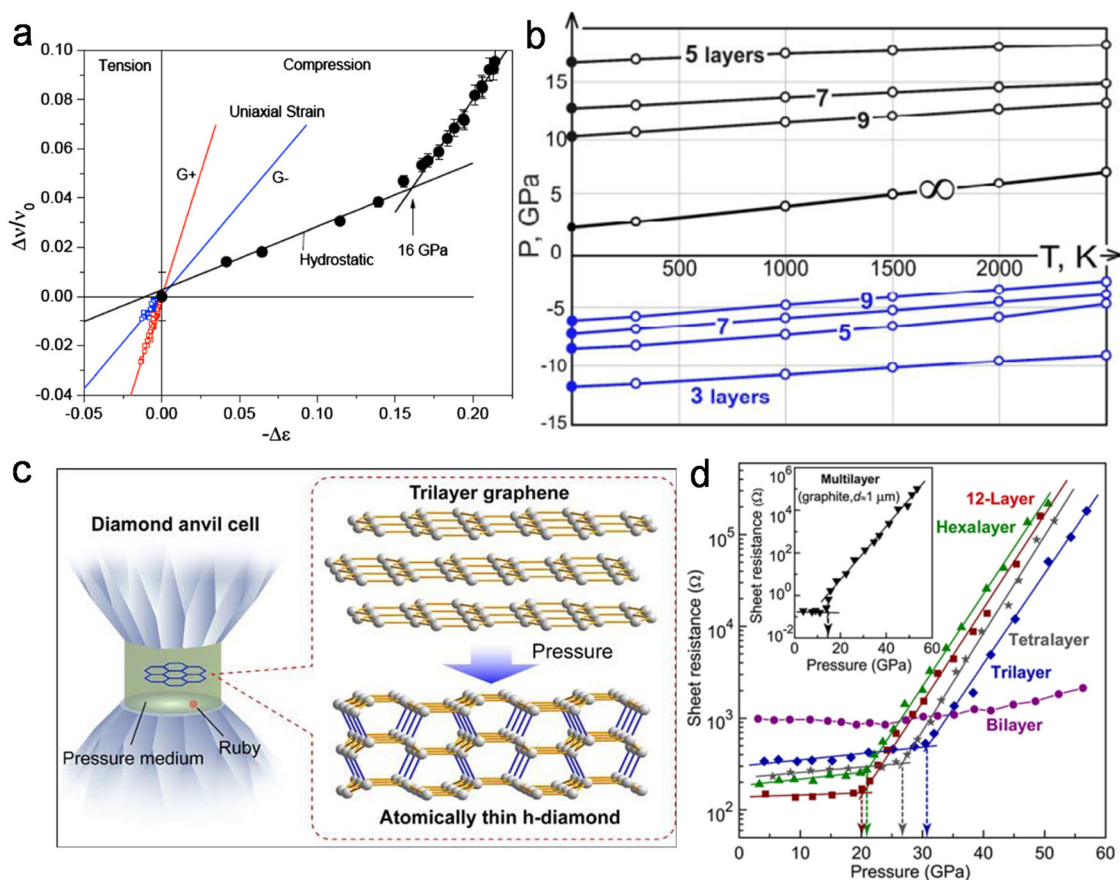
Fig. 5 Studies on the preparation of clean diamane materials. (a) Strain dependence of the normalized G-band of the present seven-layered graphene under hydrostatic compression in comparison with that measured in non-hydrostatic tension by four-point bending measurements. Reproduced with permission.[58] Copyright 2013, Elsevier B.V. (b) Phase diagram for diamond films with (110) surface. Reproduced with permission.[26] Copyright 2014, Elsevier B.V. (c) Schematic showing the diamond anvil cell and the transformation from trilayer graphene to atomically thin CD. (d) Sheet resistance *vs.* pressure curves for 12-, hexa-, tetra-, tri-, and bilayer graphene measured at room temperature. The solid lines are a guide for the eyes. The pressure dependence of the resistance of graphite is also presented as a reference for comparison (inset). Reproduced with permission.[17] Copyright 2020, the American Chemical Society.

characteristics of diamane extend its potential applications to nano-optoelectronics in tunnels, linear optical waveguides, optoelectronic sensors, and nano-electronics in low-power and miniaturized electronics. The super mechanical stiffness of diamane makes it very attractive for ultrathin protective coatings, with potential use in aerospace composites for example.[60] Because of the low friction coefficient of its hydrogenated surface, diamane was reported to be used to increase the wear resistance of coated mechanical pieces.[61] Moreover, diamane should be biocompatible to make it really relevant in bio-devices and bio-sensors, and it can be possibly used in thermal management as a result of its expected high thermal conductivity.[62] Research also shows that diamane is a better host system for single photon emission than diamond due to its lower effective Bohr radius of defects and higher radiative electronic transition state.[63] A diamane nanoribbon resonator was reported to possess a high natural frequency, high quality factor, high figure of merit, and high in-plane stiffness according to theoretical studies. Thus, compared with graphene,

which is influenced by its edge configuration, diamane would perform better than single layer/bilayer graphene, MoS_2, and other two-dimensional (2D) material-based resonators, which are appealing for high-resolution sensing applications.[64] Recently, Piazza *et al.* provided a snapshot of the main advances in the synthesis of sub-10 nm-thick sp^3-C-rich films, which include hydrogenated amorphous carbon or not, nano-crystalline diamond films, graphane, diamanes and diamanoids. In this report, the diamanes were expected to have a lower k-constant than bulk diamond ($k = 5.7$); presumably similar to that of a-C:H (in the range of 2.6–3.3). As low-k dielectric materials, diamanes can be applied to improve the performance of nano-electronic metal interconnect structures.[65]

3.1 Mechanical properties

Mechanical strength and impact resistance for are essential requirements of any material for its application. Diamane is regarded as the thinnest diamond film.[13] Thus, it is expected

to inherit many outstanding properties of diamond[66] including superior mechanical properties. In general, interlayer bonds exhibit much stronger resistance to shear, and thus influence the structural integrity of the framework.[55] The simulated indentation tests revealed the much higher in-plane stiffness of diamane than graphene and graphane (Fig. 6a).[23] Furthermore, Chernozatonskii *et al.* studied the elastic properties of diamane structures and obtained phonon dispersion, wave velocities and elastic constants using electronic band structure calculations. It was assessed that diamane possesses comparable structural stability to diamond based on the comparison of their in-plane longitudinal and transverse acoustic velocities obtained from phonon spectra.[67] Through DFT investigation, Pakornchote *et al.* found that hydrogenated BLG possesses a remarkably high resistance to in-plane plastic deformation induced by indentation, as implied by its high in-plane elastic constants comparable to that of diamond and lonsdaleite. The mechanical stability of the materials was confirmed through the fulfilment of the Born stability criteria.[68]

DFT was also adopted by Gao *et al.* to estimate the mechanical characteristics of multilayer-graphene films on SiC combined with experimental data. The results showed the reversible transformation from BLG to diamond-like structure due to the structural transformation from sp^2 to sp^3 at room temperature under the pressure of 1–10 GPa, resulting in stiffness and hardness values comparable to that of diamond (Fig. 6b).[15] In contrast, no characteristic phase change was observed with graphene films thicker than three to five layers (Fig. 6c). This is the first experimental verification that the mechanical strength of diamane may be comparable to that of bulk diamond through nano-indentation.

The functional components that control the ratio of the sp^2–sp^3 hybridization state affect the coefficient of the finite interlayer connected domain of carbon, and thus also affect the mechanical characteristics of diamane.[69] Bohayra *et al.* systematically assessed the thickness and functionalization effects on the mechanical properties of diamane nanosheets, as functionalized with H-, F-, and Cl-atoms *via* DFT simulations.[31] Fig. 6d and e show the acquired stress–strain responses of diamane nanosheets for the uniaxial loading along the armchair and zigzag edges, respectively. Analysis of the mechanical properties revealed that by increasing the number of carbon atomic layers in diamane, the elastic modulus and tensile strength increased, and the thickness dependency of the elastic modulus and tensile strength became more distinct on going from H to Cl atoms. It is clear
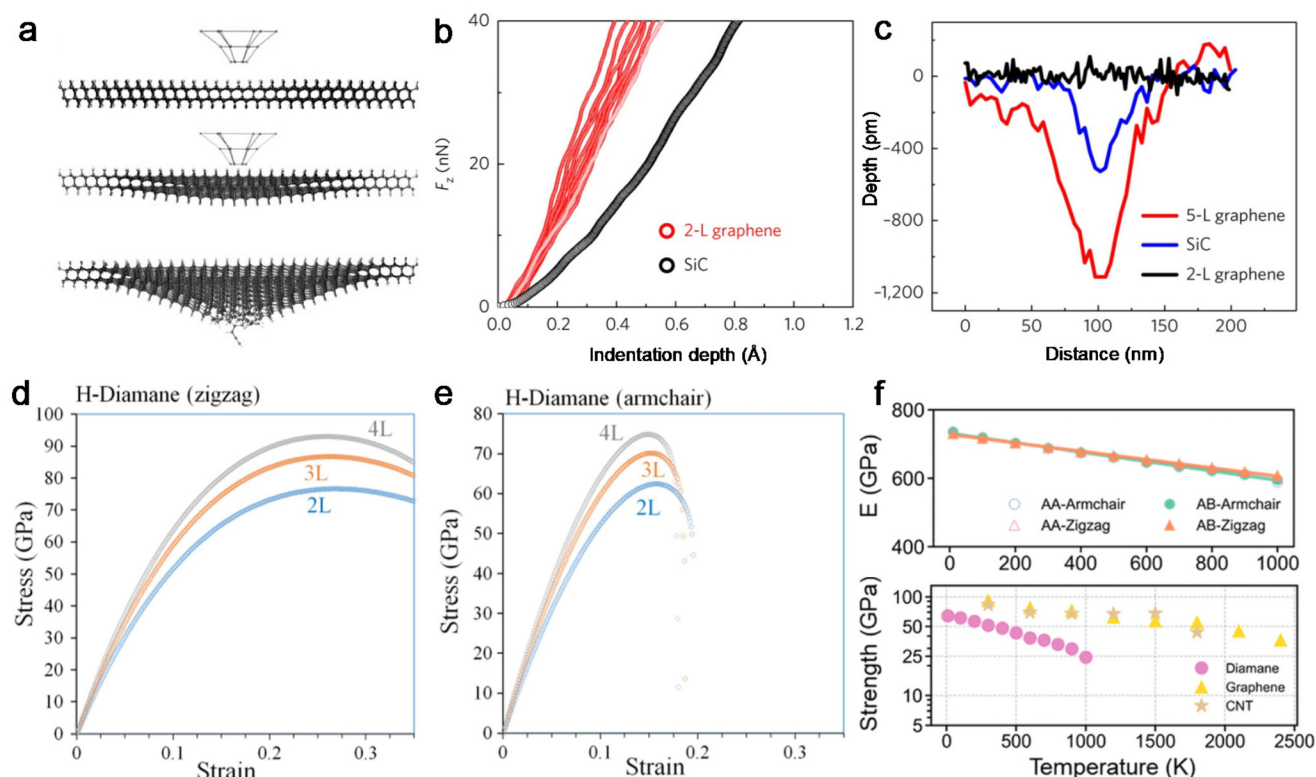
Fig. 6 Studies on the mechanical properties of diamane. (a) Molecular dynamics simulation of the deformation of the diamane membrane: initial, elastic deformation, and membrane break. Reproduced with permission.[23] Copyright 2009, Springer Nature. (b) Experimental indentation curves in 2-L epitaxial graphene (red) and SiC (black). (c) Cross-section profile of residual indents in 2-L graphene, SiC, and 5-L graphene. Reproduced with permission.[15] Copyright 2018, Springer Nature. Uniaxial stress–strain responses of H-diamane nanosheets for the uniaxial loading along armchair (d) and zigzag (e) direction. Reproduced with permission.[31] Copyright 2020, Elsevier B.V. (f) Young's moduli of D-AB and D-AA samples along the armchair and zigzag directions and fracture strength of the D-AB sample along the armchair direction as a function of temperature. Reproduced with permission.[70] Copyright 2021, the American Chemical Society.

that these novel 2D materials yield highly anisotropic tensile behavior, in which along the zigzag direction, they not only show distinctly higher tensile strengths but also keep their load-bearing ability at considerably larger strain levels. The study of the mechanical properties of diamane under tensile and bending deformation showed that the layer stacking sequence has a negligible impact on its mechanical properties.[70] These stretching and bending characteristics are different from graphene, which enables a higher opportunity for many other potential uses. Specifically, a similar Young's modulus was found along the zigzag and armchair directions, while a much greater fracture strain/strength was observed along the zigzag direction. Atomic configurations indicate that the diamane fracture is dominated by the propagation of the crack in the zigzag direction, regardless of the direction of the tensile strain. Furthermore, as the temperature increases, the relationship between the fracture strain/strength and temperature may well be outlined by the kinetic fracture theory, and the Young's modulus and the fracture strain/strength were found to decrease (Fig. 6f). These results can facilitate the essential comprehension of the mechanical behavior of diamane, which should benefit its usage in mechanic-related devices, such as mechanically stiff nano-thick elements in nanoelectronics.[70]

3.2 Electronic and electrical properties of diamane

The zero bandgap electronic structure of graphene limits its application in some advanced technologies, while the inherent semiconducting electronic nature of diamond endows it with more significant roles in the fields of electronics, optics, sensors, and possibly catalysis. Also, its considerable role in nanotechnology may be fully achieved by altering its Brillouin zone during functionalization to modulate its electronic properties. Bohayra *et al.* explored the electronic properties of 2L-H, 2L-F, 2L-Cl-diamane nanosheets by calculating their electronic band structures using the HSE06 and PBEsol functionals.[31] Fig. 7 illustrates the electronic band structures and partial density of states (CDOS) of H-, F- and Cl-diamane with different thicknesses from 2L to 4L. It was observed that 2L-diamane is a wide bandgap semiconductor with a direct gap at the Γ point with the HSE06 bandgap of 3.835 eV, while PBEsol estimated a smaller bandgap of 3.037 eV. This material is converted to a direct gap insulator with a much larger bandgap (5.655 eV) when replacing the H atoms in 2L-diamane with F atoms. There is a 3.938 eV PBEsol gap for 2L-FD, which is in accordance with the earlier PBEsol data (4.040 eV).[71] The chlorinated BLG (2L-Cl-diamane) is a direct bandgap semiconductor with an HSE06 bandgap of 2.484 eV occurring at the Γ point. Moreover, the bandgap of diamane and ClD decreases with an increase in the number of layers from 2 to 4 due to the decrease in quantum confinement effects along the normal direction to the plane of nanosheets in reports.

Thus far, the electronic structure of diamanes varies sensitively with the type of functional group and nanosheet thickness. Studies revealed that a smaller effective mass of electrons is present in diamane compared with a thick diamond film, and thus the carrier mobility in diamane may be better compared to the thickener diamond film.[72] In addition, diamane
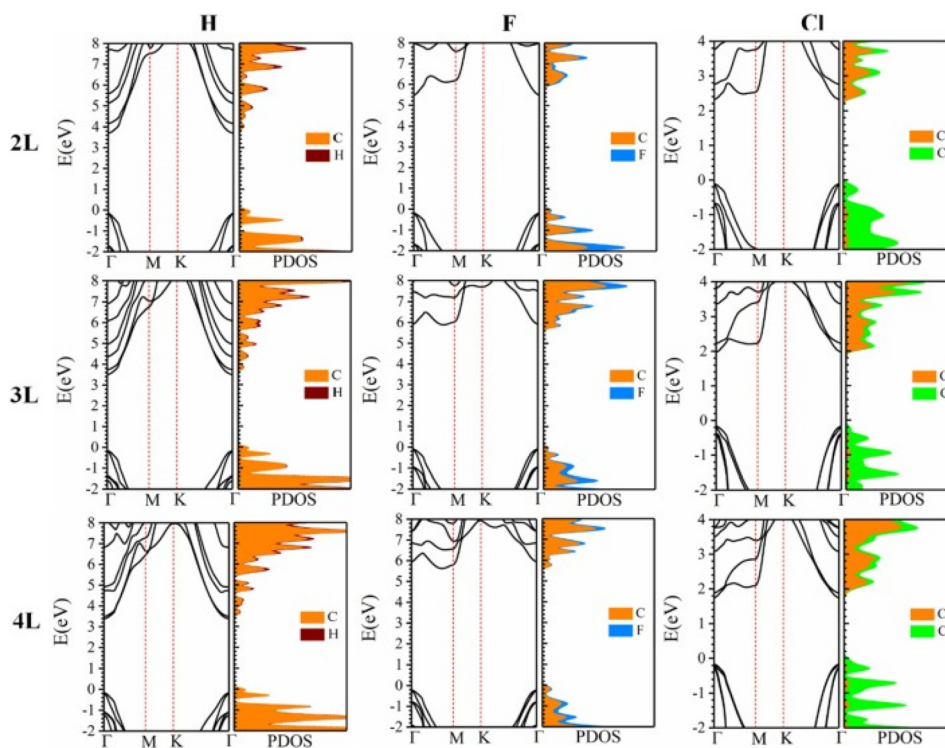

Fig. 7 Electronic band structures and total electronic density of states (DOS) of H-, F- and Cl-diamane nanosheets with different thicknesses from 2L to 4L predicted by the HSE06 functional. Reproduced with permission.[31] Copyright 2020, Elsevier B.V.

is also an excellent candidate for electrical use under extreme operating conditions, that is, high voltage, high temperature, and high frequency.[55] Exploring new 2D materials with intriguing properties can be inspired by the potential of modifying their electronic structure through functionalization, as well as the immense promise of novel electronic features that may be discovered. The electronic properties of non-Janus C_2H, C_2F, and C_2Cl diamane and their Janus counterparts of C_4HF, C_4HCl, and C_4FCl, were investigated by analyzing their electronic band structure using the PBEsol and hybrid HSE06 functionals.[49] As shown in Fig. 8, the diamane monolayers exhibit semiconducting features with a direct HSE06 (PBEsol) bandgap. Interestingly, despite some similarities between the band structures of the Janus and non-Janus monolayers (*e.g.*, band dispersions around the Fermi level), the Janus structures exhibit different bandgap values and absolute band edge positions. The relatively small direct bandgap and highly dispersed valence and conductions bands of Janus C_4HCl and C_4FCl monolayers, which are associated with very small charge carrier effective masses, make them potential materials for applications in nano-electronics devices.

In summary, unlike graphene with zero bandgap electronic character and diamond with a stable chemical structure, the adjustable bandgap of diamane depending on the film thickness and the type of functional group make it attractive for nanoelectronics, bandgap engineering in semiconductor devices, chemical nanosensors in nanocapacitors and active laser medium in nanooptics.

3.3   Thermal and optical properties of diamane

Considering that electronic devices suffer from a severe heat dissipation issue, it is highly desirable to understand the thermal transport properties of materials used in these devices. Diamond is known to be the hardest and optically transparent natural material on Earth, possessing the highest thermal conductivity of $\sim$2200 W mK^{-1} at room temperature.[66,73] The thermal conductivity is influenced by the heat transport, which is ultimately influenced by the acoustic mode and optic mode. Zhu *et al.* studied the thermal conductivity properties of diamane using the Peierls–Boltzmann transport equation, showing that the stacking sequence has an important impact on its thermal conductivity.[61] The theoretical study showed that diamane has a large thermal conductivity, which is comparable to that of diamond, mainly due to the acoustical out-of-plane (ZA) phonon modes. With hydrogen suppression on each side, BLG films with AB and AA stacking are transformed into cubic and hexagonal diamane, respectively. Intriguingly, the thermal conductivity depends the most on the stacking order, that is, the thermal conductivity of $\sim$2240 W mK^{-1} of AA-stacked diamane (D-AA) (Fig. 9a) is shown to be significantly larger than that of AB-stacked diamane at 300 K by 15% due to the limitation of phonon scattering channels by the presence of horizontal reflection symmetry. This feature is universal to many 2D materials with reflection symmetry, which is not limited to precise single atomic plane systems, for example, graphene.

To understand the impact of functional groups on the thermal transport properties of diamane, Zhu *et al.*[29] investigated the thermal transport properties of FD-AB/FD-AA and compared them to that of diamane (Fig. 9b). The thermal transport in FD is significantly suppressed, that is, the thermal conductivity of FD-AB/FD-AA is reduced by about 82% compared to diamane-AB/diamane-AA, which is reported due to the significant reduction in the contribution of acoustic modes after fluorination. Moreover, Raeisi *et al.* explored the underlying mechanisms resulting in significant effects of functional groups on the thermal conductivity of diamane nanosheets by employing machine-learning interatomic poten-
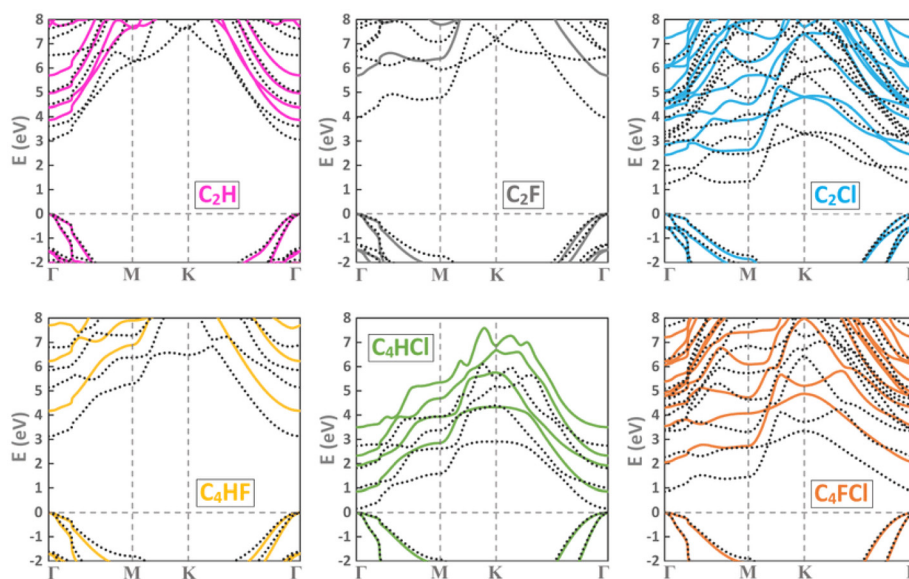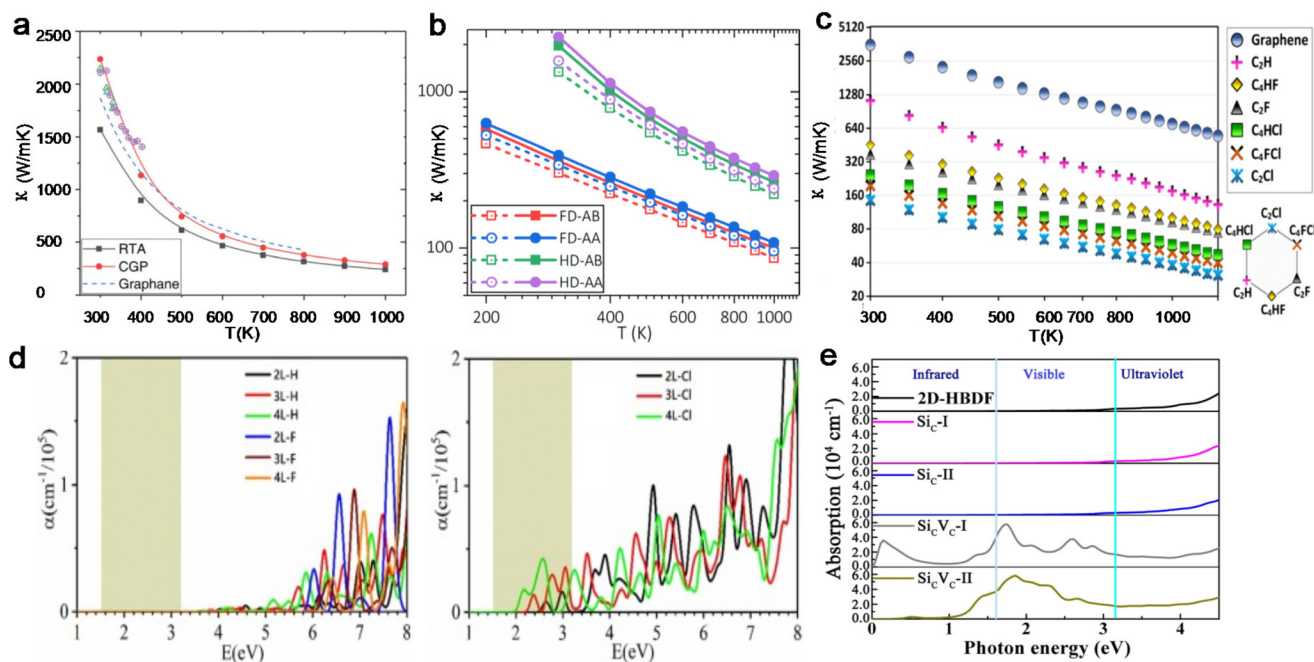

Fig. 8   Electronic band structures of diamane monolayers computed using the PBEsol (dotted lines) and hybrid HSE06 (continuous lines) methods. Reproduced with permission.[49] Copyright 2020, Elsevier B.V.

Fig. 9 (a) Thermal conductivity as a function of temperature for AA-stacked diamane (D-AA). Reproduced with permission.[61] Copyright 2019, The Royal Society of Chemistry. (b) Thermal conductivities of FD-AB (squares) and FD-AA (circles) obtained based on the relaxation time approximation (RTA) (dashed lines) and the conjugate gradient algorithm with preconditioning (CGP) (solid lines) method. The corresponding thermal conductivities in diamane-AB and diamane-AA are also shown for comparison. Reproduced with permission.[29] Copyright 2019, AIP Publishing. (c) Estimated lattice thermal conductivities as a function of temperature for non-Janus and Janus diamane. Reproduced with permission.[49] Copyright 2020, Elsevier B.V. (d) Optical absorption of diamane nanosheets predicted using the HSE06 method. (e) Absorption coefficient of the Si-doped diamane configurations. The three energy regions divided by the two vertical lines are infrared, visible, and ultraviolet. Reproduced with permission.[31] Copyright 2020, Elsevier B.V.

tials in obtaining the anharmonic force constants.[49] According to the results, the room temperature lattice thermal conductivity of graphene and non-Janus C_2H, C_2F, and C_2Cl diamane and their Janus counterparts of C_4HF, C_4HCl and C_4FCl diamane were estimated to be 3636, 1145, 377, 146, 454, 244, and 196 W mK^{-1}, respectively (Fig. 9c). It is interesting to see the thermal conductivity of the Janus diamanes fall between that of their non-Janus counterparts. Besides, the thermal conductivity of diamane can also be tuned by changing the mass of functional groups alone. Zhang *et al.* revealed the relationship between the thermal conductivities of diamane-AB/diamane-AA and the mass of hydrogen at 300 K, and found that the thermal conductivity of diamane was maximized at 1960 and 2236 W mK^{-1} for diamane-AB and diamane-AA, respectively.[74] With an increasing mass of hydrogen, the phonons in diamane are subjected to dramatic suppression and the lifetimes of acoustic phonons are appreciably shortened, resulting in a quick reduction in thermal conductivities in diamane. It is worth noting that although the thermal properties of diamanes reported in these studies do not show superiority compared to that of bulk diamond, the giant thermal conductivity together with the modulated wide bandgap and its special 2D geometry hold great promise in electronic semiconductors applications under extreme conditions, *e.g.*, high temperature.

Diamanes have extraordinary optical qualities in addition to electrical and thermal properties. In accordance with the available literature, the optical features of diamane are attributed to its large bandgap, which can be influenced by a number of external factors.[71] Its linear optical property was studied quantitatively based on the frequency-dependent complex dielectric function. The results showed that the static refractive index of diamanes (1.01–1.73) are smaller than that of bulk diamond (2.20). The low refractive index represents the faster speed of spread than in bulk diamond and the energy loss would decrease in diamanes, which can be used as optoelectronic sensors.[75] Materials made of functionalized diamanes that are clear and bendable can be utilized in nanophotonics devices.[76] In addition, the optical properties of diamane nanosheets studied by calculating their frequency-dependent absorption coefficients using the HSE06 functional indicate that diamane and FD nanosheets have no absorbance in the visible light region, but possess remarkable absorbance coefficients in the UV region, while ClD nanosheets are predicted to absorb light in a broad range of the visible region of the light spectrum and phonon dispersions (Fig. 9d). *Ab initio* molecular dynamics results confirm that the diamane, FD, and ClD nanosheets exhibit good stability.[31] Considering their good dynamical and thermal stabilities and moderate direct bandgap, Cl-diamanes may be promising candidates for opto-

electronic devices. Besides different functional groups, the optical properties of diamane can also be strongly modulated by various dopants, such as Si (Fig. 9e), P and Li and the introduction of vacancies,[75,77] endowing it with potential for application in the fields of highly active photodetectors/photocatalysts. Diamanes are considered to have superior optical capabilities because of their optical uniqueness, wide gap spectra, and numerous resonance peaks in the valent and conductivity bands in the density of states. Particularly, different functional groups can add outstanding optical qualities to this unique material through substitution or functionalization. These qualities are essential for the effective operation of various optoelectronic applications.

4.   Summary and challenges

In this review, we outlined the recent progress made in diamane and its substituents (H-, F-, Cl-, and OH-diamanes) including their development history, structure details, theoretical simulations of properties, experimental synthesis methods, and their potential applications. However, despite the intense research on 2D materials theoretically and experimentally, the complete understanding of 'diamane', a 2D nano-membrane, remains imprecise, where most of the studies carried out on diamane, diamanoid, and diamond-like thin films are theoretical and simulation-based computational methods at present.

Taking the thermal transport properties as an example, as will be readily seen when calculating the physical properties of diamanes with atomistic simulations, there are still some uncertainties and challenges, which give rise to doubts and questions among researchers, mainly due to the following reasons. Size effects: the thickness of atomically thin diamanes is just a few atoms, which has a significant impact on the way heat is transported through the material, leading to size effects that are not well understood to date. Anisotropy: similar to other 2D materials exhibiting anisotropic thermal transport, this anisotropy is challenging to calculate accurately, especially when working with different theoretical models. Interface effects: the thermal transport properties of diamanes are affected by the interfaces they form with other materials, such as substrates and other 2D materials. These interface effects are usually difficult to model and measure, leading to uncertainties in the calculated properties. In addition, there are also some experimental limitations: measuring the physical properties of diamanes is reported to be challenging, and different experimental techniques may give different results. There may also be issues with sample preparation, such as contamination and damage, which can affect the measured properties.

Therefore, although significant progress has been achieved in understanding the physical properties of diamanes, there is a great need for experiments to acquire well-defined available samples beyond the chemical functionalization and high-pressure methods (i). Besides, although the chemical transformation method is already the most commonly used way to prepare diamane-based materials, the realization of completely hydrogenated or fluorinated diamane appears challenging, which is limited by the control of the experimental conditions and the characterization capabilities (ii). Also, more sufficient evidence of the hydrogenation process of diamane should be supplemented. Specially, direct observation through techniques such as transmission electron microscopy has not been achieved due to the fact that the sp²-C to sp³-C conversion was found to be electron sensitive, even for an electron energy as low as 80 keV. New *in situ* characterization techniques can be employed in the research of diamane-formation processes (iii). With the diverse stacking sequence, composition, layers, and functional groups of graphene, the abundant structure configurations of diamane can be presented. In addition, various physical properties of different diamanes have been forecasted by theoretical simulation, which indeed still need support from persuasive normalization experiments to ascertain the predicted properties. Thus, the clarification of the structure of diamane and summary of the precursor–product–property relationship require extreme works (iv). Although preliminary research on diamane has created a high hope about its suitability for some practical applications, proposing alternative routes for the bulk production of high-quality diamane and investigating its real application possibility remain great challenges to the science community. We hope that this review can provide an in-depth comprehensive reference for further exploration and innovation on diamanes and other new carbon allotropes.

Conflicts of interest

There are no conflicts to declare.

Acknowledgements

References

1 E. H. Falcao and F. Wudl, *J. Chem. Eng. Jpn.*, 2007, **82**, 524–531.

2 J. O. Sofo, A. S. Chaudhari and G. D. Barber, *Phys. Rev. B: Condens. Matter Mater. Phys.*, 2007, **75**, 153401.

3 K. Zhang, Y. Zhang and L. Shi, *Chin. Chem. Lett.*, 2020, **31**, 1746–1756.

4 K. S. Novoselov, A. K. Geim, S. V. Morozov, D. Jiang, Y. Zhang, S. V. Dubonos, I. V. Grigorieva and A. A. Firsov, *Science*, 2004, **306**, 666–669.

5 Y. Zhang, Y.-W. Tan, H. L. Stormer and P. Kim, *Nat. Commun.*, 2005, **438**, 201–204.

6   K. S. Novoselov, Z. Jiang, Y. Zhang, S. V. Morozov, H. L. Stormer, U. Zeitler, J. C. Maan, G. S. Boebinger, P. Kim and A. K. Geim, *Science*, 2007, **315**, 1379–1379.

7   E. McCann and V. I. Fal'ko, *Phys. Rev. Lett.*, 2006, **96**, 086805.

8   Y. Cao, V. Fatemi, S. Fang, K. Watanabe, T. Taniguchi, E. Kaxiras and P. Jarillo-Herrero, *Nature*, 2018, **556**, 43–50.

9   Z. Gao, J. Li, Z. Zhang and W. Hu, *Chin. Chem. Lett.*, 2022, **33**, 2270–2280.

10 A. P. M. Barboza, M. H. D. Guimaraes, D. V. P. Massote, L. C. Campos, N. M. B. Neto, L. G. Cancado, R. G. Lacerda, H. Chacham, M. S. C. Mazzoni and B. R. A. Neves, *Adv. Mater.*, 2011, **23**, 3014–3017.

11 L.-s. Li and X. Zhao, *J. Phys. Chem. C*, 2011, **115**, 22168–22179.

12 D. Odkhuu, D. Shin, R. S. Ruoff and N. Park, *Sci. Rep.*, 2013, **3**, 3276.

13 S. Rajasekaran, F. Abild-Pedersen, H. Ogasawara, A. Nilsson and S. Kaya, *Phys. Rev. Lett.*, 2013, **111**, 085503.

14 L. G. P. Martins, M. J. S. Matos, A. R. Paschoal, P. T. C. Freire, N. F. Andrade, A. L. Aguiar, J. Kong, B. R. A. Neves, A. B. de Oliveira, M. S. C. Mazzoni, A. G. S. Filho and L. G. Cancado, *Nat. Commun.*, 2017, **8**, 96.

15 Y. Gao, T. Cao, F. Cellini, C. Berger, W. A. de Heer, E. Tosatti, E. Riedo and A. Bongiorno, *Nat. Nanotechnol.*, 2018, **13**, 133–138.

16 F. Piazza, K. Gough, M. Monthioux, P. Puech, I. Gerber, R. Wiens, G. Paredes and C. Ozoria, *Carbon*, 2019, **145**, 10–22.

17 F. Ke, L. Zhang, Y. Chen, K. Yin, C. Wang, Y.-K. Tzeng, Y. Lin, H. Dong, Z. Liu, J. S. Tse, W. L. Mao, J. Wu and B. Chen, *Nano Lett.*, 2020, **20**, 5916–5921.

18 F. Piazza, K. Cruz, M. Monthioux, P. Puech and I. Gerber, *Carbon*, 2020, **169**, 129–133.

19 F. Piazza, M. Monthioux, P. Puech and I. C. Gerber, *Carbon*, 2020, **156**, 234–241.

20 S. Wen, B. Liu, W. Li, T. Liang, X. Li, D. Yi, B. Luo, L. Zhi, D. Liu and B. Wang, *Adv. Funct. Mater.*, 2022, **32**, 2203960.

21 Z. Tao, J. Du, Z. Qi, K. Ni, S. Jiang and Y. Zhu, *Appl. Phys. Lett.*, 2020, **116**, 133101.

22 L. G. P. Martins, D. L. Silva, J. S. Smith, A.-Y. Lu, C. Su, M. Hempel, C. Occhialini, X. Ji, R. Pablo, R. S. Alencar, A. C. R. Souza, A. A. Pinto, A. B. de Oliveira, R. J. C. Batista, T. Palacios, M. S. C. Mazzoni, M. J. S. Matos, R. Comin, J. Kong and L. G. Cancado, *Carbon*, 2021, **173**, 744–757.

23 L. A. Chernozatonskii, P. B. Sorokin, A. G. Kvashnin and D. G. Kvashnin, *JETP Lett.*, 2009, **90**, 134–138.

24 O. Leenaerts, B. Partoens and F. M. Peeters, *Phys. Rev. B: Condens. Matter Mater. Phys.*, 2009, **80**, 245422.

25 L. Y. Antipina and P. B. Sorokin, *J. Phys. Chem. C*, 2015, **119**, 2828–2836.

26 A. G. Kvashnin, L. A. Chernozatonskii, B. I. Yakobson and P. B. Sorokin, *Nano Lett.*, 2014, **14**, 676–681.

27 A. Bianco, Y. Chen, Y. Chen, D. Ghoshal, R. H. Hurt, Y. A. Kim, N. Koratkar, V. Meunier and M. Terrones, *Carbon*, 2018, **132**, 785–801.

28 S. Paul and K. Momeni, *J. Phys. Chem. C*, 2019, **123**, 15751–15760.

29 L. Zhu and T. Zhang, *Appl. Phys. Lett.*, 2019, **115**, 151904.

30 P. V. Bakharev, M. Huang, M. Saxena, S. W. Lee, S. H. Joo, S. O. Park, J. Dong, D. C. Camacho-Mojica, S. Jin, Y. Kwon, M. Biswal, F. Ding, S. K. Kwak, Z. Lee and R. S. Ruoff, *Nat. Nanotechnol.*, 2020, **15**, 59–66.

31 B. Mortazavi, F. Shojaei, B. Javvaji, M. Azizi, H. Zhan, T. Rabczuk and X. Zhuang, *Appl. Surf. Sci.*, 2020, **528**, 147035.

32 J. Wang, L. Li, J. Wang, W. Yang, P. Guo, M. Li, D. Liu, H. Zeng and B. Zhao, *Nanomaterials*, 2022, **12**, 2939.

33 P. B. Sorokin and B. I. Yakobson, *Nano Lett.*, 2021, **21**, 5475–5484.

34 S. Khamkaeo, T. Pakornchote, A. Ektarawong, T. Bovornratanaruks and K. Hongo, *J. Phys.: Conf. Ser.*, 2023, **2431**, 012057.

35 L. A. Chernozatonskii, V. A. Demin and D. G. Kvashnin, *J. Phys. Chem. Lett.*, 2022, **13**, 5399–5404.

36 F. Piazza and M. Monthioux, *C—J. Carbon Res.*, 2021, **7**, 30.

37 F. Piazza, M. Monthioux, P. Puech, I. C. Gerber and K. Gough, *C—J. Carbon Res.*, 2021, **7**, 17.

38 S. K. Tiwari, R. Pandey, N. Wang, V. Kumar, O. J. Sunday, M. Bystrzejewski, Y. Zhu and Y. K. Mishra, *Adv. Sci.*, 2022, **9**, 2105770.

39 G. Qin, L. Wua and H. Gou, *Funct. Diamond*, 2021, **1**, 83–92.

40 P. R. Wallace, *Phys. Rev.*, 1947, **71**, 622–634.

41 K. S. Novoselov, A. K. Geim, S. V. Morozov, D. Jiang and Y. Zhang, *Science*, 2004, **306**, 666–669.

42 C. Fu, Z. Wang, J. Liu, H. Jiang, G. Li and C. Zhi, *Prog. Nat. Sci.*, 2016, **26**, 319–323.

43 L. A. Chernozatonskii, B. N. Mavrin and P. B. Sorokin, *Phys. Status Solidi B*, 2012, **249**, 1550–1554.

44 X. Chen, M. Dubois, S. Radescu, A. Rawal and C. Zhao, *Carbon*, 2021, **175**, 124–130.

45 J. Sung, *J. Mater. Sci.*, 2000, **35**, 6041–6054.

46 R. Z. Khaliullin, H. Eshet, T. D. Kuhne, J. Behler and M. Parrinello, *Nat. Mater.*, 2011, **10**, 693–697.

47 H. Li, J. Li, Z. Wang and G. Zou, *Chem. Phys. Lett.*, 2012, **550**, 130–133.

48 G. Kresse and J. Furthmiiller, *Comput. Mater. Sci.*, 1996, **6**, 15–50.

49 M. Raeisi, B. Mortazavi, E. V. Podryabinkin, F. Shojaei, X. Zhuang and A. V. Shapeev, *Carbon*, 2020, **167**, 51–61.

50 G. I. Csonka, J. P. Perdew, A. Ruzsinszky, P. H. T. Philipsen, S. Lebègue, J. Paier, O. A. Vydrov and J. G. Ángyán, *Phys. Rev. B: Condens. Matter Mater. Phys.*, 2009, **79**, 155107.

51 B. Silvi and A. Savin, *Nature*, 1994, **371**, 683–686.

52 A. V. Krukau, O. A. Vydrov, A. F. Izmaylov and G. E. Scuseria, *J. Chem. Phys.*, 2006, **125**, 224106.

53 H. Li, B. Liu, X. Yang, Y. Gao, X. Luo, X. Guan, Z. Zhang, Z. Yu and B. Wang, *Prog. Nat. Sci.*, 2022, **32**, 700–704.

54 J. Sivek, O. Leenaerts, B. Partoens and F. M. Peeters, *J. Phys. Chem. C*, 2012, **116**, 19240–19245.

55 T. Cheng, Z. Liu and Z. Liu, *J. Phys. Chem. C*, 2020, **8**, 13819–13826.

56 K.-J. Jeon, Z. Lee, E. Pollak, L. Moreschini, A. Bostwick, C.-M. Park, R. Mendelsberg, V. Radmilovic, R. Kostecki, T. J. Richardson and E. Rotenberg, *ACS Nano*, 2011, **5**, 1042–1046.

57 J. Son, H. Ryu, J. Kwon, S. Huang, J. Yu, J. Xu, K. Watanabe, T. Taniguchi, E. Ji, S. Lee, Y. Shin, J. H. Kim, K. Kim, A. M. v. d. Zande and G.-H. Lee, *Nano Lett.*, 2021, **21**, 891–898.

58 S. M. Clark, K.-J. Jeon, J.-Y. Chen and C.-S. Yoo, *Solid State Commun.*, 2013, **154**, 15–18.

59 A. R. Muniz and D. Maroudas, *Phys. Rev. B: Condens. Matter Mater. Phys.*, 2012, **86**, 75404.

60 R. S. Ruoff, *MRS Bull.*, 2012, **37**, 1314–1318.

61 L. Zhu, W. Li and F. Ding, *Nanoscale*, 2019, **11**, 4248–4257.

62 B. Javvaji, B. Mortazavi, X. Zhuang and T. Rabczuk, *Carbon*, 2021, **185**, 558–567.

63 S. Gupta, Ji.-H. Yang and B. I. Yakobson, *Nano Lett.*, 2019, **19**, 408–414.

64 Z. Zheng, H. Zhan, Y. Nie, X. Xu, D. Qi and Y. Gu, *Carbon*, 2020, **161**, 809–815.

65 F. Piazza, M. Monthioux and P. Puech, *Carbon Trends*, 2022, **9**, 100219.

66 C. J. H. Wort and R. S. Balmer, *Mater. Today*, 2008, **11**, 22–28.

67 L. A. Chernozatonskii, P. B. Sorokin, A. A. Kuzubov, B. P. Sorokin, A. G. Kvashnin, D. G. Kvashnin, P. V. Avramov and B. I. Yakobson, *J. Phys. Chem. C*, 2011, **115**, 132–136.

68 T. Pakornchote, A. Ektarawong, B. Alling, U. Pinsook, S. Tancharakorn, W. Busayaporn and T. Bovornratanaraks, *Carbon*, 2019, **146**, 468–475.

69 P. B. Sorokin and L. A. Chernozatonskii, *Phys.-Usp.*, 2013, **56**, 105–122.

70 Y.-C. Wu, J.-L. Shao, Z. Zheng and H. Zhan, *J. Phys. Chem. C*, 2021, **125**, 915–922.

71 F. Karlicky and M. Otyepka, *J. Chem. Theory Comput.*, 2013, **9**, 4155–4164.

72 A. G. Kvashnin and P. B. Sorokin, *J. Phys. Chem. Lett.*, 2014, **5**, 541–548.

73 X. Meng, L. Qiu, G. Xi, X. Wang and L. Guo, *SmartMat*, 2021, **2**, 466–487.

74 T. Zhang and L. Zhu, *Nanotechnology*, 2020, **31**, 435409.

75 J. Li, H. Yin, N. Gao, M. Zhang, J. Mu, L. Gao and H. Li, *Diamond Relat. Mater.*, 2019, **99**, 107526.

76 L. A. Chernozatonskii, V. A. Demin and D. G. Kvashnin, *C —J. Carbon Res.*, 2021, **7**, 17.

77 D. Qiu, Q. Wang, S. Cheng, N. Gao and H. Li, *Results Phys.*, 2019, **13**, 102240.